Available online at www.sciencedirect.com
ScienceDirect
Journal of Sound and Vibration 325 (2009) 49–68
JOURNAL OF SOUND AND VIBRATION
www.elsevier.com/locate/jsvi

# Experimental validation of an ambient vibration-based multiple damage identification method using statistical modal filtering

S. El-Ouafi Bahlous, H. Smaoui, S. El-Borgi*

*Applied Mechanics and Systems Research Laboratory, Tunisia Polytechnic School, La Marsa 2078, Tunisia*

Received 23 July 2008; received in revised form 20 February 2009; accepted 3 March 2009
Handling Editor: C.L. Morfey
Available online 2 April 2009

**Abstract**

For civil engineering structures, ambient vibration tests are preferred over forced vibration ones because the artificially excitation of large structures having low natural frequencies is quite difficult and expensive. In the ambient vibration tests, operation disturbances can be avoided and the measured response is representative of the actual operating conditions of the structures which vibrate due to natural excitation. The proposed damage identification method is intended for moderate degrees of damage and requires vibration data relative to the current and reference states of the structure as well as a parametric finite element model. It is based on a residual generated from a modal filtering approach by the calculation of the error between the measurements at the current state and their projections onto the incomplete modal basis of the structure as identified at reference state. To detect and locate damage, the residual is evaluated by means of global, sensitivity and rejection tests, modified to allow only physically feasible simple and multiple damage scenarios. The mean of the residual, which turns out to be normally distributed, is used in the final phase of damage quantification. The proposed damage diagnosis method is validated experimentally via ambient vibration tests conducted on full-scale reinforced concrete beams and slabs which contain various simple and multiple damage configurations. With damage expressed in terms of loss of flexural stiffness, the damage detection, localization and quantification are found to be successful for degrees of damage less than about 28% of the initial flexural stiffness of the tested specimens. The exception is that, for multiple damage scenarios, the relative quantification errors may be unacceptable in locations where poor accuracy is expected.


## 1. Introduction

Diagnosis of structures based on output-only, ambient vibration tests is becoming more popular nowadays [1–3]. Robust methods for finding the dynamic signature of structures from ambient vibration measurements are now available, for example, in the commercial computer code ARTeMIS Extractor [4]. The changes of the state of a structure at different times of its life cycle usually alter its dynamic signature. Comparison of the resulting signatures constitutes an important tool for the evaluation and monitoring of damage.

*Corresponding author. Tel.: +216 98 59 30 05; fax: +216 71 74 88 43.
*E-mail address:* sami.elborgi@gnet.tn (S. El-Borgi).

0022-460X/$ - see front matter © 2009 Elsevier Ltd. All rights reserved.
doi:10.1016/j.jsv.2009.03.001

A number of methods of damage assessment rely on the identification of the modal parameters of the structure before and after damage, based on output-only measurements. In these so-called modal-based methods, damage is estimated according to several criteria which may include the change in frequencies [5], mode shapes, Modal Assurance Criterion and Coordinate Modal Assurance Criterion [2,6], mode shape curvature and modal strain energy [7,8], Ritz vectors [9], stiffness and flexibility matrices [10,11]. The main disadvantage of modal methods is the loss of information due to data compression resulting from the computation of the modal parameters [1].

To overcome this disadvantage, time-domain methods may constitute an alternative to modal methods. Time-domain methods make use of vibration measurements before and after damage and evaluate appropriate residuals in terms of either the direct measured data alone or combined with identified modal parameters. Residuals can be based on: (i) auto-regressive moving-average vector, auto-regressive and auto-regressive with exogenous inputs models [12]; (ii) appropriate distance between measurements before and after damage such that the Mahalanobis distance [13], the mean strain energy measure which uses response data for a specified time period [14]; (iii) model-based state space observers where the design of damage detection filter consists of finding feedback gains and a filter output gain [15]; (iv) stochastic subspace-based identification method and a statistical local approach [16–18] and (v) statistical modal filtering (SMF) method [19].

The proposed SMF method was developed after studying the existing methods and trying to combine their advantages and eliminate their disadvantages. First, a significant aspect is the robustness of these methods on the three levels of damage identification which are the detection, the localization and the quantification of damage [1]. The robustness can be defined as the insensitivity of the methods to the measurement noise and to other errors, such as modeling errors, in cases of simple and multiple damages. In previous works, the damage quantification was not always reached and the question of robustness was not treated in a sufficiently rigorous manner. The SMF method, which is a statistical time-domain approach, is proposed for detection, localization and quantification of damage having the advantage of preserving robustness at all these levels. The robustness of such a method resides in the development of a new residual which exploits the maximum of information contained in the measurements and reduces the dependency on the model.

Secondly, the majority of existing methods allows the identification of important damage and remains not very sensitive to small levels of damage. The correct identification by the modal methods, for example, is only possible for significant changes of behavior since the detection of variations in the modal characteristics is relatively straightforward at advanced stage of degradation [2]. To overcome this problem, the proposed SMF method is developed especially for the damage identification of small changes. The evaluations are carried out within a statistical framework to distinguish the variations, compared to a reference behavior, caused by small levels of damage from those caused by other sources of errors (measurement and modeling).

Finally, damage detection and localization are based on generalized likelihood ratio (GLR) tests to which constraints were added in order to allow only physically feasible damage [19]. As for the level of damage quantification, the majority of existing methods such as Ref. [3], that manage to treat this last level, consists in solving directly an opposite problem of quantification, without enough robustness in the preceding levels, as in the updating methods. In the proposed SMF approach, the localization of damage is treated as a problem of detection rather than an opposite problem of estimation and the quantification is treated in final phase within a statistical framework.

The objectives of this paper are twofold. The first one is to enhance the damage diagnosis methodology [19] for the purpose of making it more robust especially at the localization and quantification levels for multiple damage. These improvements include a new sensitivity test for the localization of multiple damage and a more accurate damage quantification method using the residual mean. The second and more important objective of this paper is to provide an experimental validation of the proposed methodology using ambient vibration tests performed on reinforced concrete beams and slabs with artificially created damage.

This paper is organized as follows. Section 2 presents a summary of our damage diagnosis methodology while Section 3 describes the new enhancements. Section 4 is devoted to the experimental validation.

## 2. Damage diagnosis methodology

Structural health monitoring consists in confronting the signal $\mathbf{y_d}$ measured at a current state with a reference signal $\mathbf{y_0}$. Both vectors are measured at $r$ measurement points and contain measurements at $N$ different instants of time. The state of the structure can be described in its finite element model by a set of physical and/or geometrical parameters which form a vector $\boldsymbol{\theta}$ of dimension $p$. When $\boldsymbol{\theta} = \boldsymbol{\theta_0}$, the structure is at its reference state which may correspond to an undamaged state. The state defined by $\boldsymbol{\theta} = \boldsymbol{\theta_d}$ represents the current state of the structure. The monitoring of the system consists in detecting changes in the vector $\boldsymbol{\theta}$.

In the modal filtering approach, residual generation is based on the estimation of the error between the measurements taken on the structure at the current state and their projections onto the incomplete modal basis of the structure as identified at reference state [19]. This projection is represented by the following relation:

$$\overline{\mathbf{y}}_{\mathbf{t,d}} = [\boldsymbol{\Phi}(\boldsymbol{\theta_0})\boldsymbol{\Phi}^{+}(\boldsymbol{\theta_0})]\mathbf{y}_{\mathbf{t,d}} \tag{1}$$

in which $\overline{\mathbf{y}}_{\mathbf{t,d}}$ is the projection of the vector $\mathbf{y}_{\mathbf{t,d}}$ onto the modal basis $\boldsymbol{\Phi}(\boldsymbol{\theta_0})$, $\mathbf{y}_{\mathbf{t,d}}$ is the $r \times 1$ measurement vector at an instant $t$, given from the current signal $\mathbf{y_d}$, $\boldsymbol{\Phi}(\boldsymbol{\theta_0})$ is the incomplete $r \times m$ modal matrix, identified at the reference state $\boldsymbol{\theta_0}$ and, whose columns represent the $m$ lowest dominant vibration modes.

By assuming that $r \geqslant m$, the $m \times r$ matrix $\boldsymbol{\Phi}^{+}(\boldsymbol{\theta_0})$ is the pseudo-inverse of $\boldsymbol{\Phi}(\boldsymbol{\theta_0})$ which is given by $\boldsymbol{\Phi}^{+}(\boldsymbol{\theta_0}) = (\boldsymbol{\Phi}^{\mathbf{T}}(\boldsymbol{\theta_0})\boldsymbol{\Phi}(\boldsymbol{\theta_0}))^{-1}\boldsymbol{\Phi}^{\mathbf{T}}(\boldsymbol{\theta_0})$.

Therefore, the expression of the error, at an instant $t$ of measurement time, is given by

$$\boldsymbol{\varepsilon}_{\mathbf{t,d}}(\boldsymbol{\theta_0}) = \mathbf{y}_{\mathbf{t,d}} - \overline{\mathbf{y}}_{\mathbf{t,d}} = [\mathbf{I_r} - \boldsymbol{\Phi}(\boldsymbol{\theta_0})\boldsymbol{\Phi}^{+}(\boldsymbol{\theta_0})]\mathbf{y}_{\mathbf{t,d}}, \tag{2}$$

where $\mathbf{I_r}$ is the identity matrix of dimensions $r \times r$.

The error vector given by Eq. (2) represents, therefore, the response outside of the modal subspace generated by the retained vibration modes. This modal filtering is the base of the residual generation [19].

The proposed residual $\boldsymbol{\xi}$ is essentially the gradient of the average of the quadratic error $\|\boldsymbol{\varepsilon}_{\mathbf{t,d}}(\boldsymbol{\theta_0})\|^2$ between the measurements taken on the structure at the current state and their projections onto the incomplete modal basis of the reference state [19]. If the structure is undamaged (i.e., the current state and the reference state are the same), it can be easily shown that the corresponding error is minimal and its gradient evaluated at $\boldsymbol{\theta} = \boldsymbol{\theta_0}$ is approximately null. This gradient would have been equal to zero if the considered modal basis had been complete, if the model had been a perfect representation of the structure and if measurements had been free of noise. On the other hand, should the measurements represent a damaged state, the gradient and consequently the residual are different from zero. The detailed formulation of the residual is given in El-Ouafi et al. [19].

The expression of this residual $\boldsymbol{\xi}$, proposed in Ref. [19], is given by

$$\boldsymbol{\xi} = \sqrt{N}\dot{\mathbf{P}}(\boldsymbol{\theta_0})^{\mathrm{T}}(\hat{\mathbf{R}}_{\mathbf{d}} \otimes \mathbf{I_r})\mathbf{P}(\boldsymbol{\theta_0}), \tag{3}$$

where

$$\mathbf{P}(\boldsymbol{\theta}) = \mathrm{vec}(\boldsymbol{\Gamma}(\boldsymbol{\theta})), \tag{4}$$

$$\dot{\mathbf{P}}(\boldsymbol{\theta}) = \mathrm{vec}(\nabla\boldsymbol{\Gamma}(\boldsymbol{\theta})|_{\boldsymbol{\theta}}), \tag{5}$$

$$\hat{\mathbf{R}}_{\mathbf{d}} = \frac{1}{N}\sum_{t=1}^{N}\mathbf{y}_{\mathbf{t,d}}\mathbf{y}_{\mathbf{t,d}}^{\mathbf{T}} \tag{6}$$

in which $\boldsymbol{\Gamma}(\boldsymbol{\theta}) = \mathbf{I_r} - \boldsymbol{\Phi}(\boldsymbol{\theta})\boldsymbol{\Phi}^{+}(\boldsymbol{\theta})$ is an $r \times r$ matrix; the $r \times r$ matrix $\hat{\mathbf{R}}_{\mathbf{d}}$ corresponds to the current signal $\mathbf{y_d}$; the symbol $\otimes$ is the Kronecker tensor product; the operator vec( ) is a column stacking operator, it reshapes the $(r \times r)$ matrix $\boldsymbol{\Gamma}(\boldsymbol{\theta})$ to a vector $\mathbf{P}(\boldsymbol{\theta})$, of dimension $r^2 \times 1$ and the $(r \times r) \times p$ array $\nabla\boldsymbol{\Gamma}(\boldsymbol{\theta})|_{\boldsymbol{\theta}}$ to a matrix $\dot{\mathbf{P}}(\boldsymbol{\theta})$, of dimension $r^2 \times p$.

For small damage levels [17,19], $E_{\boldsymbol{\theta}_{\mathbf{d}}}(\boldsymbol{\xi})$ can be approximated by a first-order Taylor series expansion around the reference state $\boldsymbol{\theta_0}$, where $E_{\boldsymbol{\theta}_{\mathbf{d}}}$ is the expectation operator when the measurement vector is $\mathbf{y_d}$. Assuming $\boldsymbol{\theta_d} = \boldsymbol{\theta_0} + \boldsymbol{\eta}/\sqrt{N}$, this approximation, which is referred to as the local asymptotic approach [17], is given by

$$E_{\boldsymbol{\theta}_{\mathbf{d}}}(\boldsymbol{\xi}) = \mathbf{J}(\boldsymbol{\theta_0})\boldsymbol{\eta}, \tag{7}$$

where $\boldsymbol{\eta}$ is the damage parameter vector, supposed to be fixed and $\mathbf{J}(\boldsymbol{\theta}_0)$ is the $p \times p$ sensitivity matrix evaluated at $\boldsymbol{\theta} = \boldsymbol{\theta}_0$; it is given by [19]

$$\mathbf{J}(\boldsymbol{\theta}_0) = \frac{1}{\sqrt{N}} \nabla E_{\boldsymbol{\theta}}(\boldsymbol{\xi})|_{\boldsymbol{\theta}=\boldsymbol{\theta}_0}, \tag{8a}$$

$$= -[(\mathbf{P}(\boldsymbol{\theta}_0)^{\mathrm{T}}(\hat{\mathbf{R}}_0 \otimes \mathbf{I}_r)) \otimes \mathbf{I}_p]\ddot{\mathbf{P}}(\boldsymbol{\theta}_0) - \dot{\mathbf{P}}(\boldsymbol{\theta}_0)^{\mathrm{T}}(\hat{\mathbf{R}}_0 \otimes \mathbf{I}_r)\dot{\mathbf{P}}(\boldsymbol{\theta}_0) \tag{8b}$$

in which the matrix $\hat{\mathbf{R}}_0$ corresponds to the reference signal $\mathbf{y}_0$, $\hat{\mathbf{R}}_0 = 1/N \sum_{t=1}^{N} \mathbf{y}_{t,0}\mathbf{y}_{t,0}^{\mathrm{T}}$, $\mathbf{I}_p$ is the identity matrix of dimension $p \times p$ and $\ddot{\mathbf{P}}(\boldsymbol{\theta}) = \nabla(\mathrm{vec}(\dot{\mathbf{P}}(\boldsymbol{\theta})^{\mathrm{T}}))|_{\boldsymbol{\theta}}$ a matrix of size $pr^2 \times p$.

Based on the central limit theorem [20] and a local asymptotic approach [17], the residual $\boldsymbol{\xi}$ turns out to be asymptotically normally distributed ($\mathcal{N}$) with zero mean under the reference condition, nonzero mean under the damaged condition and constant covariance. Therefore, for small damage levels allowing the use of the first-order Taylor series expansion and the local asymptotic approach, the statistical test can be formulated as follows:

$$\boldsymbol{\xi} \mapsto \begin{cases} \mathcal{N}(\mathbf{0}, \boldsymbol{\Sigma}(\boldsymbol{\theta}_0)) & \text{under } H_0 \\ \mathcal{N}(\mathbf{J}(\boldsymbol{\theta}_0)\boldsymbol{\eta}, \boldsymbol{\Sigma}(\boldsymbol{\theta}_0)) & \text{under } H_1 \end{cases}, \tag{9}$$

where $\boldsymbol{\eta}$ is the damage parameter vector of size $p$, $H_0 : \boldsymbol{\eta} = \mathbf{0}$ is the null hypothesis and $H_1 : \boldsymbol{\eta} \neq \mathbf{0}$ an alternative hypothesis which describe the states of absence and presence of damage, respectively, $\boldsymbol{\Sigma}(\boldsymbol{\theta}_0)$ is the asymptotically determined covariance matrix of size $p \times p$.

The statistical test indicates the most probable hypothesis, $H_0$ or $H_1$, that can be used to provide information on damage detection based on a global test proposed by Basseville [17]. Damage localization consists of determining the nonzero components of the vector $\boldsymbol{\eta}$ based on the sensitivity and statistical rejection tests [17]. In a civil engineering structure, damage is usually reflected by a reduction in its physical and/or geometrical properties. Therefore, non-positivity constraints are imposed on the damage parameters in the detection and localization tests [19]. A flowchart of the described diagnosis methodology is shown in Fig. 1. The strategy of damage localization is to perform a test for each damage parameter, leading to a family of hypotheses pairs: $\{(H_0^i : \boldsymbol{\eta}_i = \mathbf{0}; H_1^i : \boldsymbol{\eta}_i < \mathbf{0}),\ 1 \leqslant i \leqslant p\}$. Each pair represents a parameter to be studied and the obtained results are interpreted based on the sensitivity and the statistical rejection tests. If both tests give the same location of peaks, the localization procedure is completed. Otherwise, a set of $q$ possible damage parameters ($q < p$) is selected by grouping together the results from both tests. If both test values exceed the threshold the damage is likely to be present at the corresponding location. The remaining parameters, identified only by one of the tests, are checked again using an additional test to confirm the presence or absence of damage. Details about this new test are given in Section 3.1.

In our previous work [19], damage quantification was obtained from the sensitivity and rejection tests by the expressions of the minimum of log-likelihood functions using only one dataset consisting in the entire

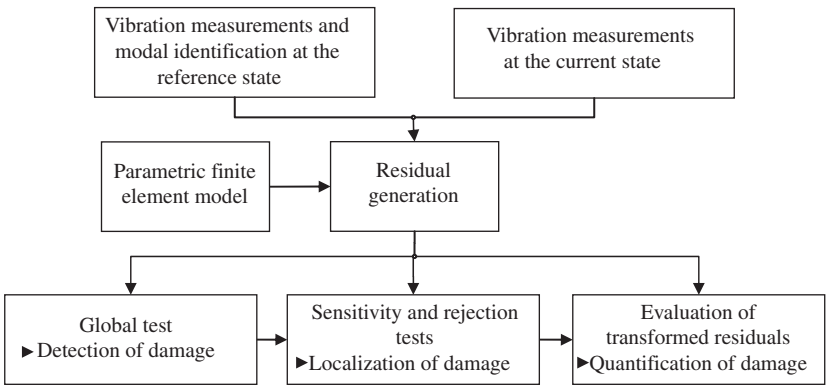


Fig. 1. Flowchart of the identification methodology.

measured signal. A more accurate estimate of the degree of damage can be determined by using several datasets corresponding to the same system measured over several time intervals. This represents one of the improvements to the proposed SMF methodology.

## 3. Enhancements of the SMF methodology

The objective of the proposed enhancements is to improve the robustness of the SMF damage diagnosis methodology especially in the localization of multiple damage and the quantification of damage in general.

### 3.1. Multiple damage localization

In order to identify multiple damage in structures, a new sensitivity test is proposed allowing detection of variations in the parameters of interest $\boldsymbol{\eta}_\mathbf{a}$, while assuming nuisance parameters $\boldsymbol{\eta}_\mathbf{b}$ to be known and not all null. The nonzero components of $\boldsymbol{\eta}_\mathbf{b}$ can be the identified parameters that reflect damage by both the sensitivity and rejection tests. The parameters of interest $\boldsymbol{\eta}_\mathbf{a}$ may contain the parameters identified by one of the tests (sensitivity and rejection tests) and not both. Similarly to our previous work [19], the damage vector $\boldsymbol{\eta}$ and the sensitivity matrix $\mathbf{J}$ may be written as follows:

$$\boldsymbol{\eta} = \begin{bmatrix} \boldsymbol{\eta}_\mathbf{a} \\ \boldsymbol{\eta}_\mathbf{b} \end{bmatrix} \tag{10a}$$

and

$$\mathbf{J} = [\mathbf{J}_\mathbf{a} \;\; \mathbf{J}_\mathbf{b}], \tag{10b}$$

where $\boldsymbol{\eta}_\mathbf{a}$ and $\boldsymbol{\eta}_\mathbf{b}$ are vectors of size $p_a$ and $p_b$, respectively ($p_a + p_b = p$).

The Fisher information matrix $\mathbf{F} = \mathbf{J}^\mathrm{T}\boldsymbol{\Sigma}^{-1}\mathbf{J}$ becomes, after injecting Eq. (10b),

$$\mathbf{F} = \begin{bmatrix} \mathbf{J}_\mathbf{a}^\mathrm{T}\boldsymbol{\Sigma}^{-1}\mathbf{J}_\mathbf{a} & \mathbf{J}_\mathbf{a}^\mathrm{T}\boldsymbol{\Sigma}^{-1}\mathbf{J}_\mathbf{b} \\ \mathbf{J}_\mathbf{b}^\mathrm{T}\boldsymbol{\Sigma}^{-1}\mathbf{J}_\mathbf{a} & \mathbf{J}_\mathbf{b}^\mathrm{T}\boldsymbol{\Sigma}^{-1}\mathbf{J}_\mathbf{b} \end{bmatrix} = \begin{bmatrix} \mathbf{F}_{\mathbf{aa}} & \mathbf{F}_{\mathbf{ab}} \\ \mathbf{F}_{\mathbf{ba}} & \mathbf{F}_{\mathbf{bb}} \end{bmatrix}. \tag{11}$$

The purpose of the new extended sensitivity test is to determine the right one between the hypotheses

$$H_0 : \boldsymbol{\eta} = \begin{bmatrix} \mathbf{0} \\ \boldsymbol{\eta}_\mathbf{b} \end{bmatrix} \quad \text{and} \quad H_1 : \boldsymbol{\eta} = \begin{bmatrix} \boldsymbol{\eta}_\mathbf{a} \\ \boldsymbol{\eta}_\mathbf{b} \end{bmatrix}, \tag{12}$$

where $\boldsymbol{\eta}_\mathbf{b}$ is a known nonzero vector, using the following GLR test:

$$\tilde{\tilde{t}}_a = 2\ln\frac{\max_{\boldsymbol{\eta}_\mathbf{a}} p_{\boldsymbol{\eta}_\mathbf{a},\boldsymbol{\eta}_\mathbf{b}}(\boldsymbol{\xi})}{p_{\mathbf{0},\boldsymbol{\eta}_\mathbf{b}}(\boldsymbol{\xi})} = l_{\mathbf{0},\boldsymbol{\eta}_\mathbf{b}}(\boldsymbol{\xi}) - \min_{\boldsymbol{\eta}_\mathbf{a}} l_{\boldsymbol{\eta}_\mathbf{a},\boldsymbol{\eta}_\mathbf{b}}(\boldsymbol{\xi}) \tag{13}$$

in which

$$\begin{aligned} l_{\boldsymbol{\eta}_\mathbf{a},\boldsymbol{\eta}_\mathbf{b}}(\boldsymbol{\xi}) &= (\boldsymbol{\xi} - \mathbf{J}\boldsymbol{\eta})^\mathrm{T}\boldsymbol{\Sigma}^{-1}(\boldsymbol{\xi} - \mathbf{J}\boldsymbol{\eta}) \\ &= \boldsymbol{\xi}^\mathrm{T}\boldsymbol{\Sigma}^{-1}\boldsymbol{\xi} - 2(\boldsymbol{\eta}_\mathbf{a}^\mathrm{T}\mathbf{J}_\mathbf{a}^\mathrm{T} + \boldsymbol{\eta}_\mathbf{b}^\mathrm{T}\mathbf{J}_\mathbf{b}^\mathrm{T})\boldsymbol{\Sigma}^{-1}\boldsymbol{\xi} + \boldsymbol{\eta}_\mathbf{a}^\mathrm{T}\mathbf{F}_{\mathbf{aa}}\boldsymbol{\eta}_\mathbf{a} + 2\boldsymbol{\eta}_\mathbf{a}^\mathrm{T}\mathbf{F}_{\mathbf{ab}}\boldsymbol{\eta}_\mathbf{b} + \boldsymbol{\eta}_\mathbf{b}^\mathrm{T}\mathbf{F}_{\mathbf{bb}}\boldsymbol{\eta}_\mathbf{b}, \end{aligned} \tag{14}$$

$$l_{\mathbf{0},\boldsymbol{\eta}_\mathbf{b}}(\boldsymbol{\xi}) = \boldsymbol{\xi}^\mathrm{T}\boldsymbol{\Sigma}^{-1}\boldsymbol{\xi} - 2\boldsymbol{\eta}_\mathbf{b}^\mathrm{T}\mathbf{J}_\mathbf{b}^\mathrm{T}\boldsymbol{\Sigma}^{-1}\boldsymbol{\xi} + \boldsymbol{\eta}_\mathbf{b}^\mathrm{T}\mathbf{F}_{\mathbf{bb}}\boldsymbol{\eta}_\mathbf{b}. \tag{15}$$

In order to evaluate the test statistic in Eq. (13), the log-likelihood function $l_{\boldsymbol{\eta}_\mathbf{a},\boldsymbol{\eta}_\mathbf{b}}(\boldsymbol{\xi})$ has to be minimized with respect to $\boldsymbol{\eta}_\mathbf{a}$, resulting in the following condition:

$$\boldsymbol{\eta}_\mathbf{a} = \mathbf{F}_{\mathbf{aa}}^{-1}(\mathbf{J}_\mathbf{a}^\mathrm{T}\boldsymbol{\Sigma}^{-1}\boldsymbol{\xi} - \mathbf{F}_{\mathbf{ab}}\boldsymbol{\eta}_\mathbf{b}). \tag{16}$$

Substituting Eq. (13) into Eq. (10), the test statistic $\tilde{\tilde{t}}_a$ can be written as

$$\tilde{\tilde{t}}_a = (\mathbf{J}_\mathbf{a}^\mathrm{T}\boldsymbol{\Sigma}^{-1}\boldsymbol{\xi} - \mathbf{F}_{\mathbf{ab}}\boldsymbol{\eta}_\mathbf{b})^\mathrm{T}\mathbf{F}_{\mathbf{aa}}^{-1}(\mathbf{J}_\mathbf{a}^\mathrm{T}\boldsymbol{\Sigma}^{-1}\boldsymbol{\xi} - \mathbf{F}_{\mathbf{ab}}\boldsymbol{\eta}_\mathbf{b}). \tag{17}$$

Using the transformed variable

$$\boldsymbol{\xi}_{\mathbf{a}}^{*} = \mathbf{J}_{\mathbf{a}}^{\mathbf{T}}\boldsymbol{\Sigma}^{-1}\boldsymbol{\xi} - \mathbf{F}_{\mathbf{ab}}\boldsymbol{\eta}_{\mathbf{b}} \tag{18}$$

which is normally distributed under $\boldsymbol{\eta}_{\mathbf{a}} \neq \mathbf{0}$ as

$$\boldsymbol{\xi}_{\mathbf{a}}^{*} \mapsto \mathcal{N}(\mathbf{F}_{\mathbf{aa}}\boldsymbol{\eta}_{\mathbf{a}}, \mathbf{F}_{\mathbf{aa}}) \tag{19}$$

the new test statistic can, finally, be written as

$$\tilde{\tilde{t}}_a = \boldsymbol{\xi}_{\mathbf{a}}^{*\mathbf{T}}\mathbf{F}_{\mathbf{aa}}^{-1}\boldsymbol{\xi}_{\mathbf{a}}^{*}. \tag{20}$$

The test statistic $\tilde{\tilde{t}}_a$ is distributed as a $\chi^2$ random variable with $p_a$ degrees of freedom (dof) and noncentrality parameter $\boldsymbol{\eta}_{\mathbf{a}}^{\mathbf{T}}\mathbf{F}_{\mathbf{aa}}\boldsymbol{\eta}_{\mathbf{a}}$.

The diagnosis is carried out by the following rule: when $\tilde{\tilde{t}}_a \geqslant \lambda$, $H_0$ is rejected, $\lambda$ being a threshold value determined from the $\chi^2$ table according to the desired Type I error rate $\alpha$ [20]. Otherwise, $\tilde{\tilde{t}}_a < \lambda$, which leads to the acceptance of $H_0$.

Similarly to the global, sensitivity and rejection tests [19], the feasibility condition on the damage parameters can be incorporated in the evaluation of the test $\tilde{\tilde{t}}_a$. This can be carried out by minimizing the quadratic function given in Eq. (14) subject to the non-positivity constraints, leading to the following expression:

$$(\mathbf{F}_{\mathbf{aa}}\boldsymbol{\eta}_{\mathbf{a}} - \mathbf{J}_{\mathbf{a}}^{\mathbf{T}}\boldsymbol{\Sigma}^{-1}\boldsymbol{\xi} + \mathbf{F}_{\mathbf{ab}}\boldsymbol{\eta}_{\mathbf{b}})\bar{\upsilon}_{\mathbf{a}} = \mathbf{0}, \tag{21}$$

where $\bar{\upsilon}_{\mathbf{a}}$ is the matrix representation of square roots of $\boldsymbol{\eta}_{\mathbf{a}}$, $\boldsymbol{\eta}_{\mathbf{a}} = -\bar{\upsilon}_{\mathbf{a}}\upsilon_{\mathbf{a}}$. It should be noted that, generally in the procedure of search of multiple damage, $\bar{\upsilon}_{\mathbf{a}}$ is one dimensional. Consequently, Eq. (21) either yields directly that $\bar{\upsilon}_{\mathbf{a}} = \mathbf{0}$ or provides a result similar to that of the test in Eq. (20).

### 3.2. Damage quantification

In previous work [19] the damage identification was conducted using the measurements of a single dataset. Based on the idea that more information can be extracted from the system under study by generating more datasets, an attempt is made to improve the accuracy of the damage quantification results by modifying the methodology to treat several datasets instead of a single one. This is performed by first developing a transformed residual which contains information about the placement of the damaged parameters. This transformed residual is derived from the normally distributed residual $\boldsymbol{\xi} \mapsto \mathcal{N}(\mathbf{J}\boldsymbol{\eta}, \boldsymbol{\Sigma})$. Knowing the nonzero components of the damage parameter $\boldsymbol{\eta}$, i.e. those which form the vector $\boldsymbol{\eta}_{\mathbf{a}}$, the transformed residual

$$\hat{\boldsymbol{\xi}}_{\mathbf{a}} = \mathbf{J}_{\mathbf{a}}^{\mathbf{T}}\boldsymbol{\Sigma}^{-1}\boldsymbol{\xi} \tag{22}$$

is normally distributed with a nonzero mean in the damaged condition,

$$\hat{\boldsymbol{\xi}}_{\mathbf{a}} \mapsto \mathcal{N}(\mathbf{F}_{\mathbf{aa}}\boldsymbol{\eta}_{\mathbf{a}}, \mathbf{F}_{\mathbf{aa}}), \tag{23}$$

where $\mathbf{F}_{\mathbf{aa}} = \mathbf{J}_{\mathbf{a}}^{\mathbf{T}}\boldsymbol{\Sigma}^{-1}\mathbf{J}_{\mathbf{a}}$.

An estimation of the damage quantification $\hat{\boldsymbol{\eta}}_{\mathbf{a}}$ can be obtained by multiplying the transformed residual $\hat{\boldsymbol{\xi}}_{\mathbf{a}}$ by $\mathbf{F}_{\mathbf{aa}}^{-1}$,

$$\hat{\boldsymbol{\eta}}_{\mathbf{a}} = \mathbf{F}_{\mathbf{aa}}^{-1}\hat{\boldsymbol{\xi}}_{\mathbf{a}} \mapsto \mathcal{N}(\boldsymbol{\eta}_{\mathbf{a}}, \mathbf{F}_{\mathbf{aa}}^{-1}). \tag{24}$$

The average of the variables $\hat{\boldsymbol{\eta}}_{\mathbf{a}}$ estimated for several datasets gives the value of the degree of damage $\boldsymbol{\eta}_{\mathbf{a}}$,

$$\boldsymbol{\eta}_{\mathbf{a}} = E_{\theta_{\mathbf{d}}}(\hat{\boldsymbol{\eta}}_{\mathbf{a}}) = \mathbf{F}_{\mathbf{aa}}^{-1}E_{\theta_{\mathbf{d}}}(\hat{\boldsymbol{\xi}}_{\mathbf{a}}). \tag{25}$$

The damage quantification error can be estimated by computing the variance of $\hat{\boldsymbol{\eta}}_{\mathbf{a}}$ which is equal to the reciprocal of the submatrix $\mathbf{F}_{\mathbf{aa}}$ of the Fisher information matrix,

$$\mathrm{Var}(\hat{\boldsymbol{\eta}}_{\mathbf{a}}) = \mathbf{F}_{\mathbf{aa}}^{-1}\mathrm{Var}(\hat{\boldsymbol{\xi}}_{\mathbf{a}})\mathbf{F}_{\mathbf{aa}}^{-1} = \mathbf{F}_{\mathbf{aa}}^{-1}. \tag{26}$$

A detailed flowchart of the enhanced SMF diagnosis methodology is given in Appendix A.

## 4. Experimental validation on reinforced concrete elements

This study provides an experimental verification of the identification approach via ambient vibration tests conducted on reinforced concrete beams and slabs in which artificial damage is created.

### 4.1. Description of test specimens

Reinforced concrete beams and slabs were fabricated in the laboratory for the purpose of experimentally validating the proposed modal filtering damage diagnosis method. Various damage scenarios were created in these specimens to study simple and multiple damages with various degrees of damage.

Two beams, labeled B1 and B2, are prepared for the study. Both beams are simply supported. They have the same length and width, $l = 4.00\,\text{m}$, $w = 0.15\,\text{m}$ and have, respectively, the height $h = 0.08$ and $0.06\,\text{m}$. A photograph of the beams is shown in Fig. 2. These dimensions are chosen such that the lower natural frequencies are as close as possible to those typically found in concrete bridges. Ease of fabrication, handling constraints and damage scenarios were also determining factors in choosing these dimensions and in designing the steel reinforcement. The latter has been strictly limited to lower longitudinal bars, given that the beams are not expected to undergo reverse bending or significant shearing action. For both beams four HA type, 10 mm diameter steel bars formed the bottom row of the reinforcement. The concrete beam equivalent cross-section is calculated assuming that the lower part of the beam, subjected to tension, contributes to the stiffness as long as the allowable tensile stress is not reached. Thus the moment of inertia is estimated at $I_{B1} = 8.34 \times 10^{-6}\,\text{m}^4$ for B1 (resp. $I_{B2} = 3.00 \times 10^{-6}\,\text{m}^4$ for B2). The concrete elasticity modulus, $E = 29.5\,\text{GPa}$, is determined from conventional compression tests. The stiffness is consequently estimated at $EI_{B1} = 246.03\,\text{KN m}^2$ for B1 (resp. $EI_{B2} = 88.50\,\text{KN m}^2$ for B2).

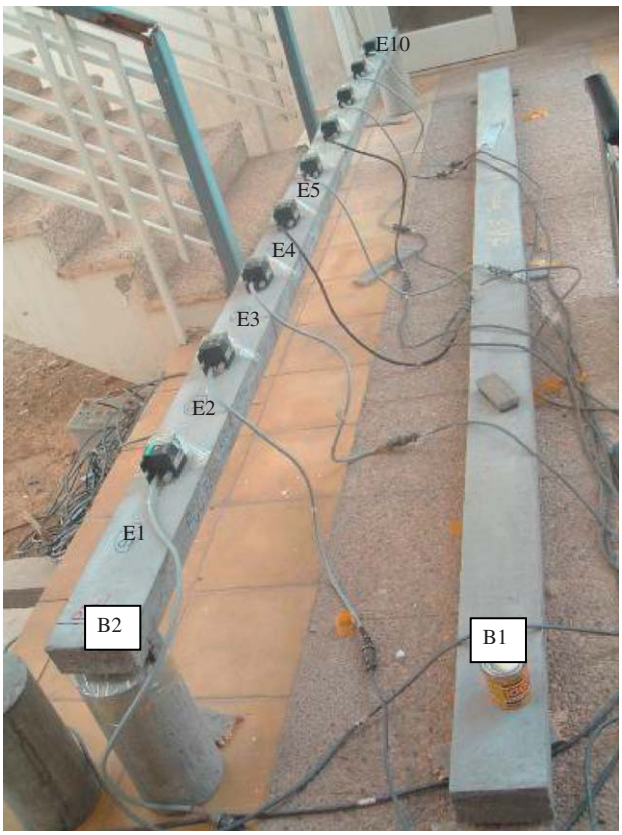


Fig. 2. Photograph of the reinforced concrete beams.

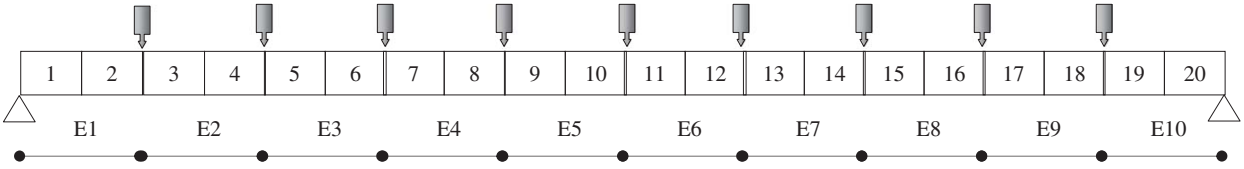


Fig. 3. Discretized beam model and placement of sensors.

Fig. 4. Damage creation in case of scenario B1-2.

The finite element model of the beam consists of 20 beam elements. Each pair of adjacent elements corresponds to a group ($E_j, j = 1, \ldots, 10$) which is characterized by the same damage parameter (Fig. 3). The considered parameters, forming the vector $\boldsymbol{\theta}$, are the stiffness $EI$ of the ten element groups.

Three damage scenarios, performed on beam B1, served in testing the identification by varying the degree of damage. The first scenario, B1-1, was created by cutting a 1 cm deep groove all over the two lateral surfaces of element group E3. Then the same grooves are made 2 cm deep, which defines scenario B1-2. Scenario B1-3 is generated by cutting an additional 0.3 cm deep groove all over the upper surface of the same element group E3. Beam B2 served to assess identification in the presence of multiple damage. Thus, damage consisted of 1 cm deep grooves cut all over the two lateral surfaces of element group E3 for scenario B2-1, then extended to element group E4 for scenario B2-2 and finally to element group E10 for scenario B2-3. Fig. 4 shows the groove cutting operation.

The grooves cause a local reduction in the stiffness $EI$ of the beam. The actual degree of damage $D_a$, expressed in terms of reduction in stiffness and the actual flexural stiffness $EI_a$ are given in Table 1 for the considered scenarios. It should be noted that, in order to avoid variation in mass due to material loss, the mass of removed concrete is replaced by an equal added mass placed on the beam. This is due to the fact that the mass is not taken into account as a parameter in the model for the presented application.

The slabs are of dimensions 2 m × 1 m. The thickness of the first slab, labeled S1, is 0.06 m and that of the second slab, S2, is 0.05 m. A photograph of the slabs is shown in Fig. 5. The reinforcement is limited to TSHA type steel bars of 4 mm diameter, with a spacing of 0.15 m. For the slab S1, the moment of inertia is estimated at $I_{S1} = 1.848 \times 10^{-5}\,\mathrm{m}^3$ per unit width (resp. $I_{S2} = 1.067 \times 10^{-5}\,\mathrm{m}^3$ for S2) and, consequently, the stiffness is estimated at $EI_{S1} = 545.292\,\mathrm{KN\,m}$ for S1 (resp. $EI_{S2} = 314.709\,\mathrm{KN\,m}$ for S2). The slabs are supported on their four corners. Finite element models of the slabs were built using 60 shell elements with three dof per node (i.e., one vertical translation and two rotations per node). The elements are grouped into 15 quadruplets

Table 1
Actual damage in beams.

| Scenario | Element group | $D_a$ (%) | $EI_a$ (KN m$^2$) |
|---|---|---|---|
| (*a*) *Damage in beam B1* | | | |
| B1-1 | E3 | 10.1 | 221.181 |
| B1-2 | E3 | 20.3 | 196.086 |
| B1-3 | E3 | 27.7 | 177.880 |
| (*b*) *Damage in beam B2* | | | |
| B2-1 | E3 | 9.4 | 80.181 |
| B2-2 | E3 | 9.4 | 80.181 |
| | E4 | 9.4 | 80.181 |
| B2-3 | E3 | 9.4 | 80.181 |
| | E4 | 9.4 | 80.181 |
| | E10 | 9.4 | 80.181 |

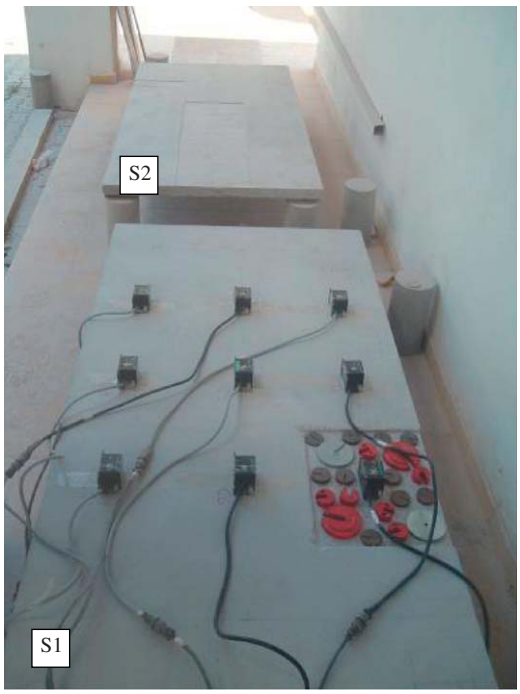


Fig. 5. Reinforced concrete slabs and measurement equipment.

($E_j$, $j = 1, \ldots, 15$) of adjacent elements. A schematic representation of the slab finite element model is illustrated in Fig. 6.

Three damage scenarios were produced for each slab. In slab S1, damage was created by cutting a 0.5, 1 cm then 1.5 cm deep groove all over the upper surface of element group E14 which define scenario S1-1, S1-2 and S1-3, respectively. In slab S2, damage was created by cutting a 0.5 cm deep groove all over the upper surface of element group E2, then extending it to element group E8 and finally to element group E9. These constitute damage scenarios S2-1, S2-2 and S2-3, respectively. The degrees of damage $D_a$, expressed in terms of reduction in stiffness per unit width and the actual flexural stiffness $EI_a$ are summarized in Table 2.

As for the beams, slab S1 was used for studying the influence of degree of damage and S2 for assessing the performance of the identification method in the presence of multiple damage.

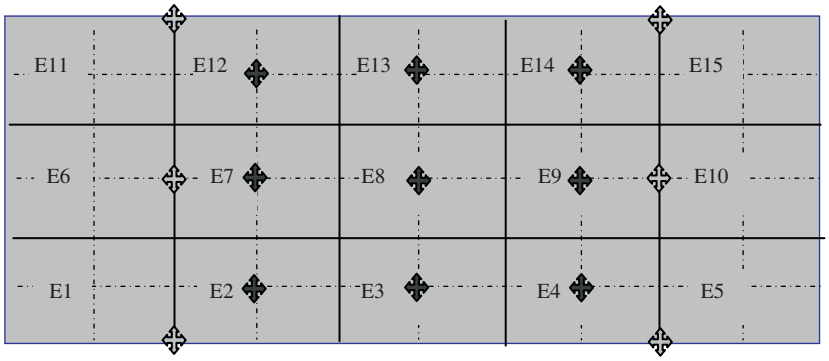


Fig. 6. Discretized shell model and placement of sensors (setup 1, setup 2).

Table 2
Actual damage in slabs.

| Scenario | Element group | $D_a$ (%) | $EI_a$ (KN m) |
|---|---|---|---|
| (*a*) *Damage in slab S1* | | | |
| S1-1 | E14 | 21.1 | 430.235 |
| S1-2 | E14 | 35.1 | 353.894 |
| S1-3 | E14 | 43.5 | 308.090 |
| (*b*) *Damage in slab S2* | | | |
| S2-1 | E2 | 24.5 | 237.605 |
| S2-2 | E2 | 24.5 | 237.605 |
| | E8 | 24.5 | 237.605 |
| S2-3 | E2 | 24.5 | 237.605 |
| | E8 | 24.5 | 237.605 |
| | E9 | 24.5 | 237.605 |

### 4.2. Description of vibration equipment and test planning

Ambient vibration tests were conducted on the structures using a sixteen-channel data acquisition system (Vibration Survey System Model VSS-3000, Kinemetrics, 1997) with nine force-balance uniaxial accelerometers (model FBA-ES-U, Kinemetrics, 2000). The sensors, which are capable of measuring accelerations of up to $\pm 0.25g$ with a resolution of 0.1 μg, convert the physical excitation into electrical signals. Cables were used to transmit the electronic signals from sensors to the signal conditioner which was used to improve the quality of the signals by removing undesired frequency contents (filtering) and amplifying the signals. The amplified and filtered analog signals were converted to digital data using a 16-bit resolution analog-to-digital converter at a speed of 1024 kHz prior to storing on the data acquisition computer. The analog-to-digital converter is capable of sampling up to sixteen channels at sampling frequencies between 0.2 and 2000 Hz. The accelerometers are capable of measuring frequencies less than 200 Hz. The ambient vibration tests were carried out on the beams and the slabs in their undamaged and damaged states. The structures were excited both artificially by a hammer applied randomly and naturally through wind and micro-tremors.

For each damage scenario, accelerations due to ambient vibration are measured at a sampling frequency of 1000 Hz during a measurement period of 6 min. This interval is divided into 18 datasets of 20 000 points each. A sample of the acceleration data is given in Fig. 7.

The accelerometers were mounted on the beam specimens at equally spaced locations as shown in Fig. 2. For the slabs, fifteen sensors were mounted on each specimen as illustrated in Fig. 6. Furthermore, since the number of accelerometers (9) was less than the number of measurements (15), the vibration measurement campaign was divided into 2 test setups, each lasting 6 min. Each setup consisted of three reference

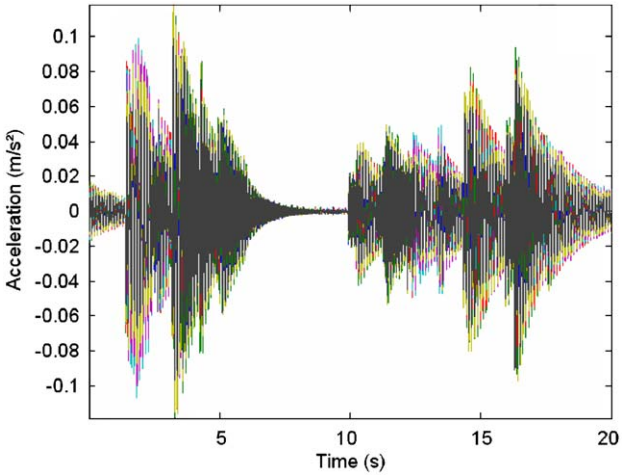


Fig. 7. Example of data for beam B1 (scenario B1-1).

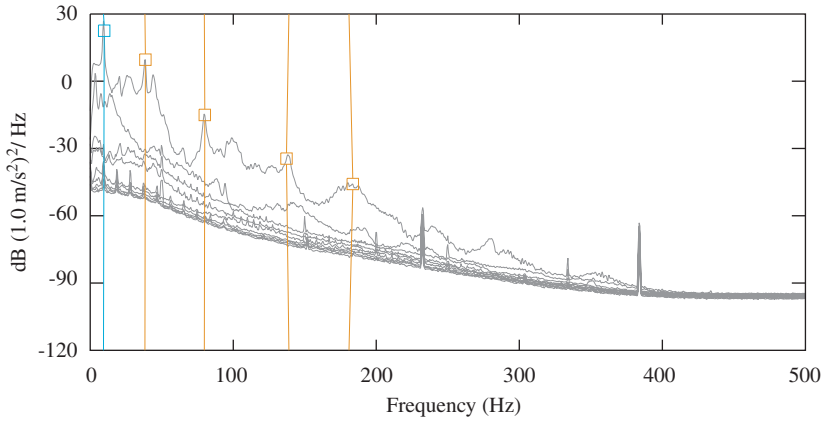


Fig. 8. Average of normalized singular values of spectral density matrices using the EFDD technique.

accelerometers which remained in their position throughout the campaign and the remaining sensors were moved to cover all the measurement points.

### 4.3. Results and discussion

#### 4.3.1. Damage identification in beams

The enhanced frequency-domain decomposition (EFDD) technique [21,22], implemented in the code ARTeMIS Extractor [4], was used to identify the modal signature of the beams. Fig. 8 shows the average of singular values of spectral density matrices using the EFDD technique. The singular values in this plot correspond to the detected frequencies. The first three lowest and dominant detected frequencies are 9.32, 38.24 and 79.74 Hz and, therefore, their corresponding modes shapes are retained for the subsequent damage identification task. It should be noted that the first three natural frequencies of the finite element model are 9.42, 37.71 and 84.86 Hz, which indicates that the modeling error is less than 6.42% in the identification of frequencies. The measurement-based mode shapes for the three detected modes are shown in Figs. 9(a)–(c). The values of the Modal Assurance Criterion MAC [1] are estimated to predict the level of correspondence between the experimental and computed finite element mode shapes. The diagonal and off-diagonal terms of the MAC matrix vary from 99.13% to 99.98% and 0.00% to 0.07%, respectively. Comparison of frequencies and mode shapes indicates an almost a one-to-one correspondence between the experimental and computed

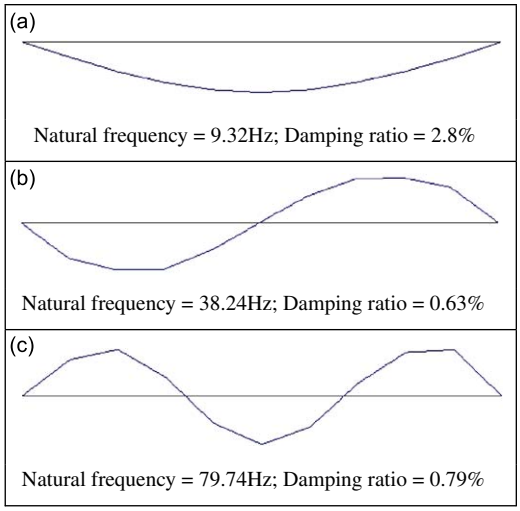


Fig. 9. Measurement-based mode shapes identified using the EFDD technique of beam B1: (a) first measured mode shape, (b) second measured mode shape and (c) third measured mode shape.

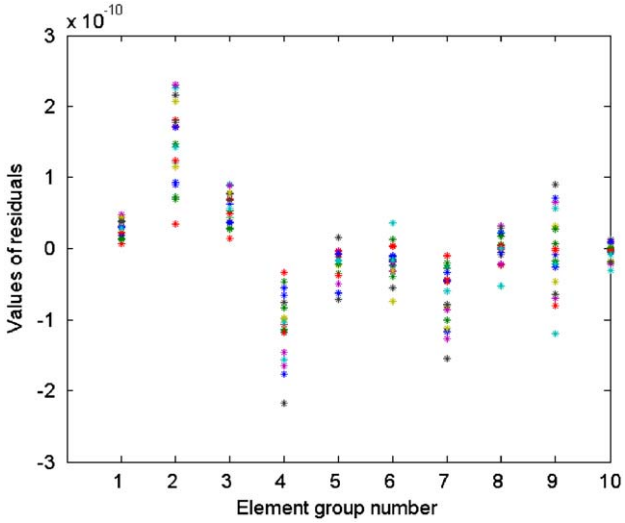


Fig. 10. Residuals calculated for the 18 datasets (B1-1).

vibration modes. As a result, it can be concluded that the finite element model of the beam reproduces reasonably well the real behavior of the undamaged structure.

The results obtained from the three damage scenarios relative to beam B1 are presented hereafter, with the objective of validating the identification with respect to the degree of damage. Since the basis of the proposed SMF method is the estimation of residual vectors which are given by Eq. (3). Fig. 10 shows an example of such quantities estimated from the eighteen datasets generated for the particular case of damage scenario B1-1. It can be seen that the mean value of the residual vectors is different from zero, which indicates that the structure may be damaged. A definite conclusion can only be made after subsequent statistical tests related to damage identification are executed.

Results of damage identification for the three damage scenarios (B1-1, B1-2 and B1-3) are summarized in Table 3. The second column of this table gives the global detection test value based on the first dataset, which follows a $\chi^2$ random variable with $p$ dof corresponding to the number of parameters in the structure. For scenario B1-1, the global test is equal to 112.0, which is much larger than the threshold value of 23.2, taken

Table 3
Damage identification results for beam B1.

| Scenario | Damage detection | Damage localization | | | Damage quantification | | Stiffness $EI$ | |
|---|---|---|---|---|---|---|---|---|
| | Value of global test | Value of sensitivity test | Value of rejection test | Damage location | $D_c$ (%) | $e_1$ (%) | $EI_c$ (KN m$^2$) | $e_2$ (%) |
| (1) | (2) | (3) | (4) | (5) | (6) | (7) | (8) | (9) |
| B1-1 | 112.0 | 67.4 | 57.3 | E3 | 10.6 | 5.0 | 219.951 | 0.6 |
| B1-2 | 233.8 | 184.1 | 118.9 | E3 | 19.1 | 5.9 | 199.038 | 1.5 |
| B1-3 | 436.3 | 302.5 | 272.8 | E3 | 20.5 | 26.0 | 195.594 | 10.0 |

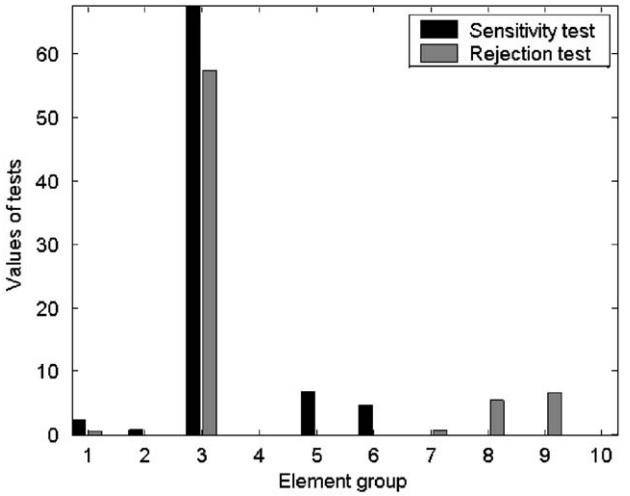


Fig. 11. Values of damage localization tests for scenario B1-1.

from $\chi^2$ table for $p = 10$ dofs and a significance level $\alpha = 1\%$ [20], which confirms the occurrence of damage and concludes the detection level. Damage localization sensitivity and rejection tests are then performed based on the first dataset by considering the ten parameters one by one, as displayed in Fig. 11, the parameters being the stiffness $EI$ of all the element groups. The threshold value of 6.63 discriminates damaged from undamaged elements, for a single dof ($p = 1$) and $\alpha = 1\%$. The values of these tests which are larger than the threshold value are those corresponding to element group E3, which are also reported numerically in columns 3 and 4 of Table 3. It is clear from Fig. 11 that the proposed SMF method correctly predicts the localization of damage in the third element group. The same conclusions are reached for damage detection and localization based on the remaining datasets. Using the mean of the calculated residuals shown in Fig. 10, the quantification of damage is estimated at 10.6% for damage scenario B1-1 (column 6 of Table 3) based on all datasets, which is close to the actual damage value of 10.1% reported in Table 1. The relative error $e_1$, between actual ($D_a$) and computed ($D_c$) degree of damage, is reported in column 7 of Table 3 and is expressed in percentage as follows: $e_1(\%) = |D_a - D_c|/D_a \times 100$ in which $D_c$ is given in column (6) of the considered Table. In addition, the relative error $e_2$, between actual ($EI_a$) and computed ($EI_c$) stiffness (column 8 of Table 3), is given in column 9 of Table 3 and is expressed in percentage as follows: $e_2(\%) = |EI_a - EI_c|/EI_a \times 100$. For the first damage scenario, the resulting relative error ($e_1$) is of the order of 5% and the corresponding relative error ($e_2$) between the actual and computed stiffness is less than 1%.

For the second and third damage scenarios (B1-2 and B1-3), all the obtained global tests are larger than the threshold value of 23.2, e.g. 233.8 and 436.3 for B1-2 and B1-3, respectively, using the first dataset (column 2

Table 4
Damage identification results for beam B2.

| Scenario | Damage detection | Damage localization | | | Damage quantification | | Stiffness $EI$ | |
|---|---|---|---|---|---|---|---|---|
| | Value of global test | Value of sensitivity test | Value of rejection test | Damage location | $D_c$ (%) | $e_1$ (%) | $EI_c$ (KN m$^2$) | $e_2$ (%) |
| (1) | (2) | (3) | (4) | (5) | (6) | (7) | (8) | (9) |
| B2-1 | 172.2 | 50.9 | 51.5 | E3 | 11.9 | 26.6 | 77.969 | 2.8 |
| B2-2 | 293.7 | 124.9 | 50.4 | E4 | 11.3 | 20.2 | 78.500 | 2.1 |
| | | 74.2 | – | E3 | 8.7 | 7.4 | 80.801 | 0.8 |
| B2-3 | 934.6 | 405.1 | 178.6 | E4 | 17.6 | 87.2 | 72.924 | 9.1 |
| | | 285.7 | | E3 | 10.2 | 8.5 | 79.473 | 0.9 |
| | | 55.1 | | E10 | 32.9 | 250.0 | 59.383 | 25.9 |
| | | 12.1 | | E5 | 2.4 | – | 86.376 | 2.4 |

of Table 3). This proves existence of damage in the beam. The only values, of the damage localization sensitivity and rejection tests, which are larger than the threshold value, are always obtained in element group E3. The quantification is achieved with a relative error, between the actual and computed degree of damage, in the order of 5.9% and 26% for the second and third scenarios, respectively (column 7 of Table 3). The corresponding relative errors between the actual and computed stiffness are 1.5% and 10% for the second and third scenarios, respectively (column 9 of Table 3). It can, therefore, be concluded that, for the case of beams, damage existence and localization were correctly predicted while the errors in the damage quantification were rather acceptable for degrees of actual damage less than 27.7% (Table 1a). Finally, it can be concluded that, based on the damage scenarios B1-1, B1-2 and B1-3, the damage quantification relative error increases for larger values of the damage and this is understandable since the proposed SMF method is based on the assumption of small damage.

The purpose of damage scenarios relative to the second beam B2 is to validate the identification with respect to multiple damage. For this beam, the first three identified natural frequencies of the undamaged state are 6.44, 26.48 and 58.71 Hz. Similarly to beam B1, the finite element model of beam B2 also reproduces reasonably well the actual behavior of the undamaged structure.

Results of damage identification for the three damage scenarios (B2-1, B2-2 and B2-3) are reported in Table 4. The second column of this table gives the detection global test value based on the first dataset. In scenario B2-1, the global test is 172.2 and sensitivity and rejection tests are 50.9 and 51.5, respectively, for element group E3 and they are less than the threshold value of 6.63 in all the others elements. Thus, damage is located correctly and the degree of damage is found to be 11.9%.

In scenario B2-2, the results, given in Fig. 12, indicate that damage occurs in multiple element groups and can be located at element groups E3, E4 and/or E5 according to the sensitivity test and at groups E3, E4 and/or E7 based on the statistical rejection test. Now the analysis is restricted to these four potential damage locations. The tree of the branch-and-bound search [19,23] leading to localization is displayed in Fig. 13 with the values of the sensitivity test at the tree nodes. One can note that, from the first level of the tree, the largest test statistic $\tilde{\tilde{t}}_{a1}$(E4) is chosen for further refinement. In the second level, using the new sensitivity test (Section 3.1) which takes into account the damage identified at the previous level, the largest test statistic $\tilde{\tilde{t}}_{a2}$(E3) is chosen for further refinement. It is interesting to mention that, in pursuing the test to the third level, the value of the test $\tilde{\tilde{t}}_{a3}$(E7) is 5.1 which is less than the threshold value of 6.63. This clearly suggests absence of damage in group E7. To conclude this example, the most probable hypothesis is that of damage occurring in groups E3 and E4, which is the actual localization. The resulting degree of damage is equal to 8.7% for element group E3 and 11.3% for E4.

In the third scenario, B2-3, based on the sensitivity and rejection tests, the possibly damaged elements are E3, E4, E5, E7, E9 and/or E10 as presented in Fig. 14 using the first dataset. The search tree leading to the localization is given in Fig. 15. The obtained degrees of damage are equal to 10.2% for element group E3,

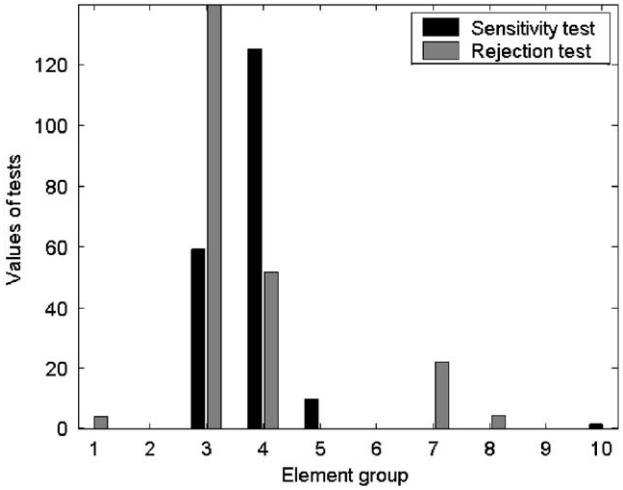


Fig. 12. Values of damage localization tests for scenario B2-2.

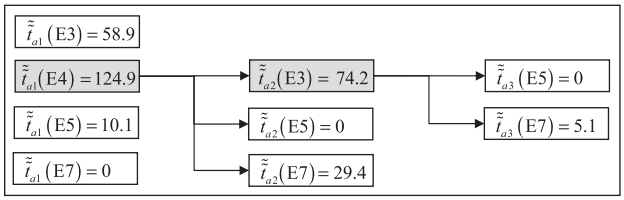


Fig. 13. Localization search tree with sensitivity test values at the nodes (scenario B2-2).

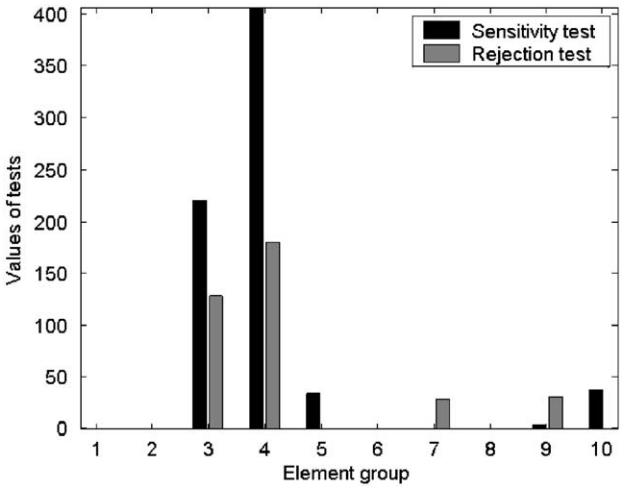


Fig. 14. Values of damage localization tests for scenario B2-3.

17.6% for E4, 2.4% for E5 and 32.9% for E10. The results of localization are acceptable because the calculated degree of damage in E5 is too small to consider the element to be undamaged. However, the performance of the quantification deteriorates with respect to element group E10. The latter is near the support and the corresponding diagonal term in the Fisher information matrix is small, as indicated in Fig. 16 and as a result the predictions is subject to large uncertainty.

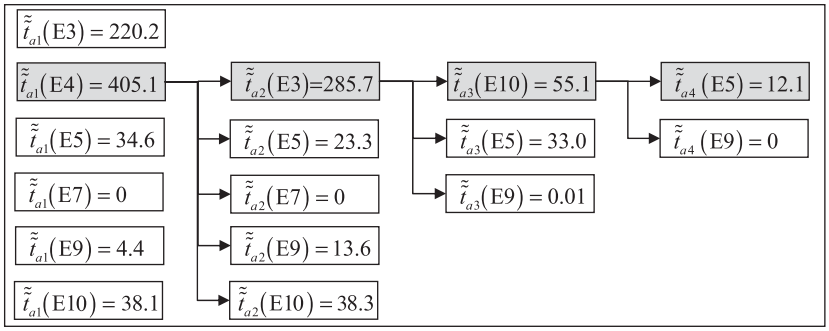


Fig. 15. Localization search tree with sensitivity test values at the nodes (scenario B2-3).

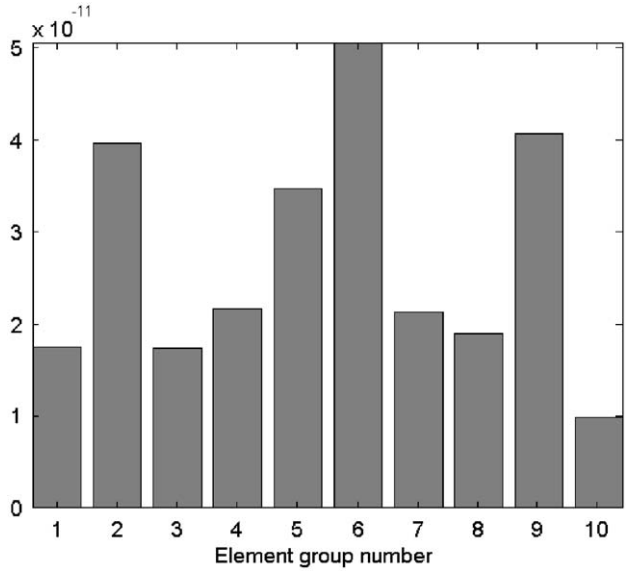


Fig. 16. Diagonal terms of Fisher information matrix for the undamaged beam B2 using nine sensors.

### 4.3.2. *Damage identification in slabs*

Similarly to the beams, three vibration modes were detected in the slabs using the EFDD technique, which correspond to the dominant modes with the lowest frequencies 27.63, 71.96 and 84.57 Hz. The first three computed frequencies are 25.11, 76.93 and 88.09 Hz which corresponds to modeling errors less than 9.1% in the identification of frequencies. The measurement-based mode shapes are shown in Figs. 17(a)–(c). The values of the Modal Assurance Criterion MAC [1] are estimated to predict the level of correspondence between the experimental and computed finite element mode shapes. The diagonal and off-diagonal terms of the MAC matrix vary from 84.5% to 99.7% and 0.03% to 14%, respectively. As a result, it can be concluded that the finite element model of the slab reproduces reasonably the real behavior of the undamaged structure.

For the three damage scenarios, the obtained global tests are larger than the threshold, which proves the existence of damage (Table 5). For scenarios S1-1 and S1-3, the maximum values of the sensitivity tests are obtained in element E14. For the scenario S1-2, the maximum values of the tests are relative to element E15 in the first level of the search tree and to element E14 in the second level. The damage is, therefore, distributed between the actual damaged element E14 and the neighboring element E15. Clearly, damage detection and localization are reasonably predicted for the three scenarios S1-1, S1-2 and S1-3, while quantification results are judged reasonable for the scenario S1-1 with a relative quantification error in the order of 11% (column 7, Table 5).

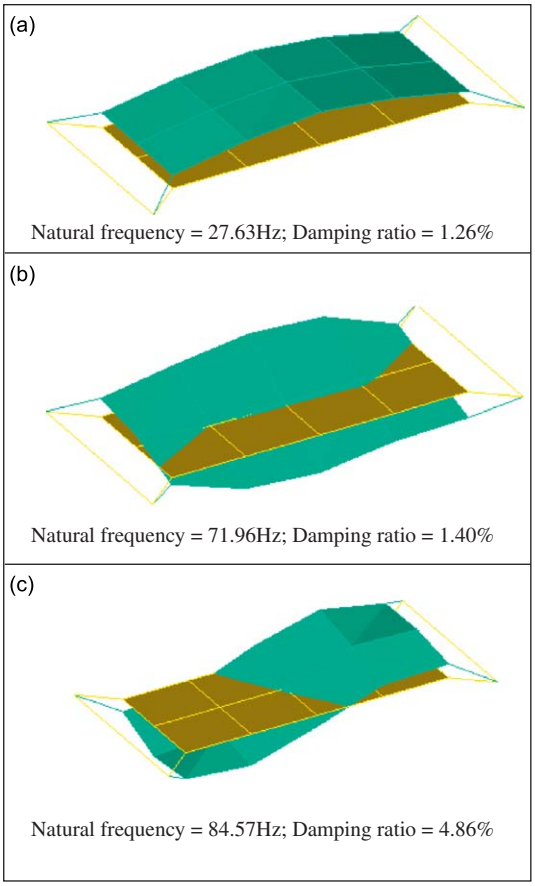


Fig. 17. Experimental mode shapes of the slab S1 using the EFDD technique: (a) first measured mode shape, (b) second measured mode shape and (c) third measured mode shape.

Table 5
Identification results for slab S1.

| Scenario | Damage detection | Damage localization | | | Damage quantification | | Stiffness $EI$ | |
|---|---|---|---|---|---|---|---|---|
| | Value of global test | Value of sensitivity test | Value of rejection test | Damage location | $D_c$ (%) | $e_1$ (%) | $EI_c$ (KN m) | $e_2$ (%) |
| (1) | (2) | (3) | (4) | (5) | (6) | (7) | (8) | (9) |
| S1-1 | 949 | 521 | 436 | E14 | 18.8 | 10.9 | 442.777 | 2.9 |
| | | 29 | | E12 | 2.7 | – | 530.569 | 2.7 |
| S1-2 | 1374 | 471 | 169 | E15 | 15.6 | – | 460.226 | 15.6 |
| | | 204 | | E14 | 13.4 | 61.8 | 472.223 | 33.4 |
| S1-3 | 2081 | 701 | 623 | E14 | 20.7 | 52.4 | 432.417 | 40.4 |
| | | 127 | | E15 | 16.0 | – | 458.045 | 16.0 |

The purpose of damage scenarios relative to the second slab S2 is to validate the identification with respect to multiple damage. The first three identified natural frequencies of the undamaged slab S2 are 20.21, 52.88 and 67.10 Hz. Similarly to slab S1, the finite element model of slab S2 also reproduces reasonably the actual behavior of the undamaged structure.

Results of the damage identification for the three damage scenarios (S2-1, S2-2 and S2-3) are reported in Table 6. The second column of this table gives the detection global test value based on the first dataset.

Table 6
Identification results for slab S2.

| Scenario | Damage detection | Damage localization | | | Damage quantification | | Stiffness $EI$ | |
|---|---|---|---|---|---|---|---|---|
| | Value of global test | Value of sensitivity test | Value of rejection test | Damage location | $D_c$ (%) | $e_1$ (%) | $EI_c$ (KN m) | $e_2$ (%) |
| (1) | (2) | (3) | (4) | (5) | (6) | (7) | (8) | (9) |
| S2-1 | 960 | 43.6 | 32.1 | E2 | 17.0 | 30.6 | 261.208 | 9.9 |
| S2-2 | 1586 | 178.5 | 159.3 | E8 | 33.1 | 35.1 | 210.540 | 11.4 |
| | | 51.9 | | E2 | 33.6 | 37.1 | 208.967 | 12.1 |
| | | 13.7 | | E1 | 3.4 | – | 304.009 | 3.4 |
| S2-3 | 1071 | 71.6 | 204.6 | E2 | 31.8 | 29.8 | 214.632 | 9.7 |
| | | 96.7 | | E8 | 24.6 | 0.4 | 237.291 | 0.1 |
| | | 32.8 | | E9 | 8.1 | 66.9 | 289.218 | 21.7 |

The calculated values of this test indicate existence of damage. The sensitivity and rejection test values are given in columns 3 and 4 of Table 6, respectively. It should be noted that the sensitivity test values are further refined using the tree of the branch-and-bound search. In scenario S2-1 where the actual damage is 24.5% and located in element group E2 (Table 2), the SMF method correctly predicted the damaged element group with a degree of damage equal to 17% (column 6 of Table 6). The resulting relative error is 30.6% and the corresponding relative error between the actual and computed stiffness is less than 10% (columns 7 and 9 of Table 3).

For scenario S2-2, where the actual damage amounts to 24.5% and is located in element groups E2 and E8 (Table 2), the SMF method predicted element groups E2, E8 and E1 to be damaged (column 6 of Table 6). Results wrongly suggest element group E1 to be damaged. Indeed, it should be noted that the truncation and the approach used in estimating the covariance matrix may introduce some errors in test values, which can be slightly larger than the threshold for an undamaged element. Since the degree of damage for this element is rather small (3.4%), the element can be considered to be undamaged. For scenario S2-3 where the actual damage is 24.5% and is located in element groups E2, E8 and E9 (Table 2), using the sensitivity and rejection tests, the damaged elements turn out to be correctly located as indicated in Table 6 (column 5).

## 5. Conclusion

The statistical modal filtering (SMF) method, proposed by the authors in Ref. [19], is enhanced for the purpose of making it more robust especially in the localization of multiple damage and in the quantification of simple and multiple damage. These improvements include a new sensitivity test for the case of multiple damage used in damage identification phases and a more accurate damage quantification method using the residual mean. The method is then validated experimentally using ambient vibration tests performed in the laboratory on reinforced concrete beams and slabs with artificial damage scenarios. These scenarios include cases of simple and multiple damage with various degrees of damage. Detection and localization are reasonably predicted for the beams and slabs. The damage quantification results are generally acceptable for degrees of damage less than 28%, corresponding to a relative error with respect to the actual stiffness in the order of 10%. However, diagnosis deteriorates as damage level increases, which is predictable since the proposed method is based on the assumption of small damage. For the case of multiple damage, the detection and localization are successfully predicted and the relative quantification errors are generally acceptable except for the case where poor accuracy is expected on the basis of the Fisher information matrix.

For real structures with many unknowns, the computational cost of the SMF method becomes too expensive in the level of damage localization. Therefore, the method may be combined with a genetic algorithm to solve the problem of damage localization in a moderate computational time, in particular when the number of damage parameters becomes significant. In Ref. [24], the proposed method was applied on a real bridge in order to demonstrate its feasibility.

**Acknowledgments**

The authors are grateful for the funding provided to their laboratory by the Tunisian Ministry of Higher Education, Scientific Research and Technology.

## Appendix A. Detailed flowchart of the enhanced SMF identification methodology

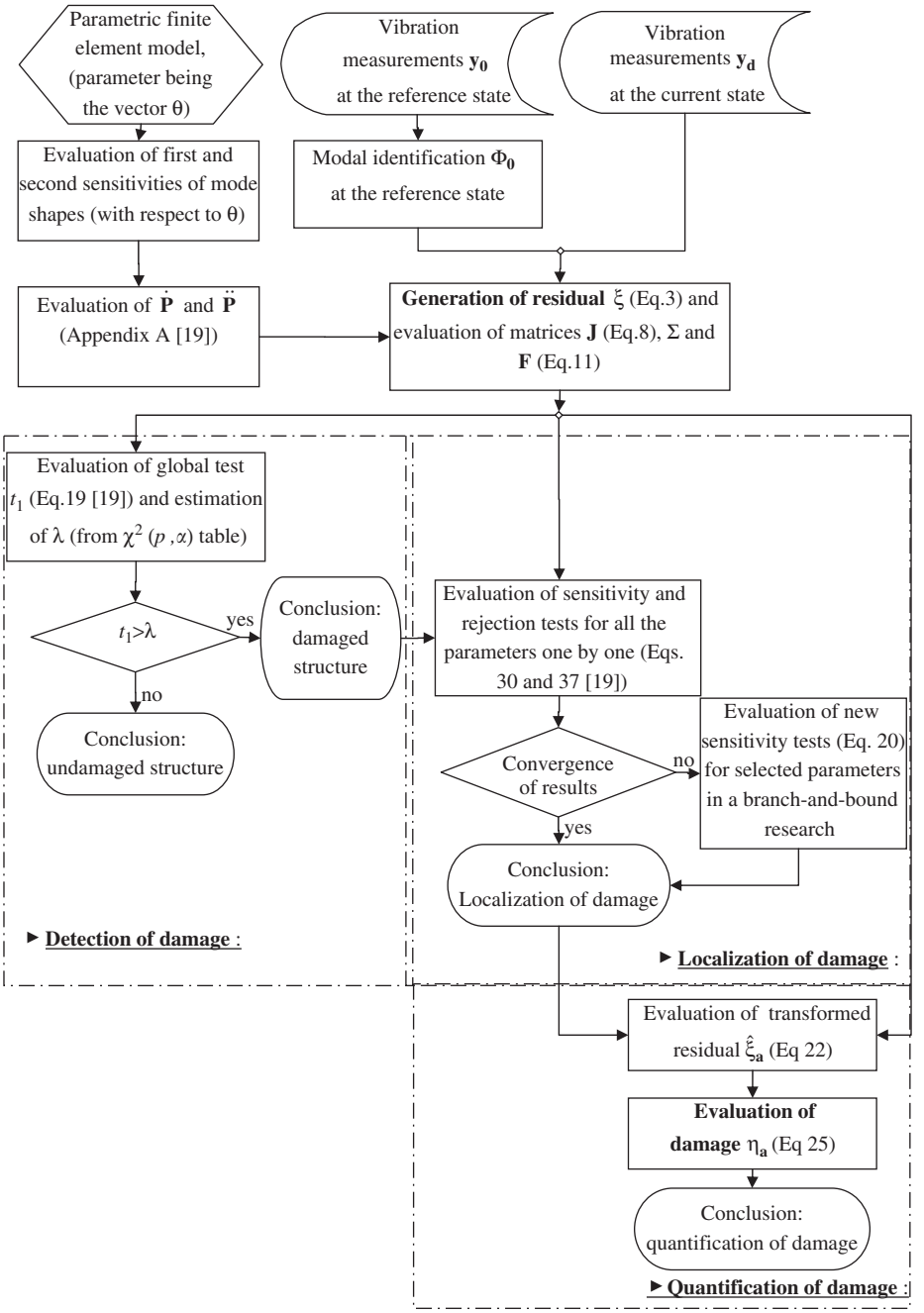

## References


[1] S.W. Doebling, C.R. Farrar, M.B. Prime, A summary review of vibration-based damage identification methods, *Shock and Vibration Digest* 30 (1998) 91–105.

[2] C.R. Farrar, D.A. Jauregui, Comparative study of damage identification algorithms applied to a bridge: I. Experiment, *Smart Materials and Structures* 7 (1998) 704–719.

[3] J.F. Lord, C.E. Ventura, E. Dascotte, Automated model updating using ambient vibration data from a 48-storey building in Vancouver, *Proceedings of the 22nd International Modal Analysis Conference*, 2004.

[4] ARTeMIS Program Overview, 〈http://www.svibs.com〉, 2007 (accessed 09.01.07).

[5] Y.S. Lee, M.J. Chung, A study on crack detection using eigenfrequency test data, *Computers and Structures* 77 (2000) 327–342.

[6] E. Viola, L. Federici, L. Nobile, Detection of crack location using cracked beam element method for structural analysis, *Theoretical and Applied Fracture Mechanics* 36 (2001) 23–35.

[7] Z.Y. Shi, S. Law, L.M. Zhang, Structural damage localization from modal strain energy change, *Journal of Sound and Vibration* 218 (1998) 825–844.

[8] T.A. Duffey, S.W. Doebling, C.R. Farrar, W.E. Baker, W.H. Rhee, Vibration-based damage identification in structures exhibiting axial and torsional response, *Journal of Vibration and Acoustics* 123 (2001) 84–91.

[9] H. Sohn, K.H. Law, Application of load-dependent Ritz vectors to Bayesian probabilistic damage detection, *Probabilistic Engineering Mechanics* 15 (2000) 139–153.

[10] D. Bernal, Damage localization using load vectors, *European COST F3 Conference*, Vol. I, Madrid, 2000, pp. 223–231.

[11] M.I. Friswell, D.J. Inman, D.F. Pilkey, The direct updating of damping and stiffness matrices, *AIAA Journal* 36 (1998) 491–493.

[12] J.B. Bodeux, J.C. Golinval, Application of ARMAV models to the identification and damage detection of mechanical and civil engineering structures, *Smart Materials and Structures* 10 (2001) 479–489.

[13] K. Worden, G. Manson, N.R.J. Fieller, Damage detection using outlier analysis, *Journal of Sound and Vibration* 229 (2000) 647–667.

[14] S. Choi, N. Stubbs, Damage identification in structures using the time-domain response, *Journal of Sound and Vibration* 275 (2004) 577–590.

[15] S.J. Kranock, L.D. Peterson, Real-time structural damage detection using model-based observers, PhD Thesis, Department of Aerospace Engineering Science, College of Engineering, University of Colorado, 2000.

[16] M. Abdelghani, M. Basseville, A. Benveniste, In-operation damage monitoring and diagnostics of vibrating structures, with applications to offshore structures and rotating machinery, *Proceedings of the 15th International Modal Analysis Conference*, Orlando, FL, 1997, pp. 1815–1822.

[17] M. Basseville, Information criteria for residual generation and fault detection and isolation, *Automatica* 33 (1997) 783–803.

[18] M. Basseville, L. Mevel, M. Goursat, Statistical model-based damage detection and localization: subspace-based residuals and damage-to-noise sensitivity ratios, *Journal of Sound and Vibration* 275 (2003) 769–794.

[19] S. El-Ouafi Bahlous, M. Abdelghani, H. Smaoui, S. El-Borgi, A modal filtering and statistical approach for damage detection and diagnosis in structures using ambient vibrations measurements, *Journal of Vibration and Control* 13 (2007) 281–308.

[20] E.J. Dudewicz, S.N. Mishra, Modern mathematical statistics, in: *Probability and Mathematical Statistics*, Wiley, New York, 1998.

[21] R. Brincker, C. Ventura, P. Andersen, Damping estimation by frequency domain decomposition, *Proceedings of the 19th International Modal Analysis Conference*, Kissimmee, FL, USA, 2001.

[22] S. El-Borgi, S. Choura, C. Ventura, M. Baccouch, F. Cherif, Modal identification and model updating of a reinforced concrete bridge, *International Journal of Smart Structures and Systems* 1 (2005) 83–101.

[23] H. Sohn, K.H. Law, A Bayesian probabilistic approach for structure damage detection, *Earthquake Engineering and Structural Dynamics* 26 (1997) 1259–1281.

[24] S. El-Ouafi Bahlous, H. Smaoui, S. El-Borgi, Ambient vibration based damage diagnosis using statistical modal filtering method and genetic algorithm: case of Beni Khiar Bridge, *Proceedings of the Fourth International Conference on Advances in Mechanical Engineering and Mechanics*, Tunisia, 16–18 December 2008.